Improved DOA estimation of MEMS vector hydrophone combined with CEEMDAN and wavelet transform for noise reduction

Zican Chang, Guojun Zhang, Wenqing Zhang, Yabo Zhang, Li Jia and Zhengyu Bai
North University of China, Taiyuan, China, and

Wendong Zhang
State Key Laboratory of Dynamic Measurement Technology, North University of China, Taiyuan, China

Abstract

Purpose – Ciliated microelectromechanical system (MEMS) vector hydrophones pick up sound signals through Wheatstone bridge in cross beam-ciliated microstructures to achieve information transmission. This paper aims to overcome the complexity and variability of the marine environment and achieve accurate location of targets. In this paper, a new method for ocean noise denoising based on improved complete ensemble empirical mode decomposition with adaptive noise combined with wavelet threshold processing method (CEEMDAN-WT) is proposed.

Design/methodology/approach – Based on the CEEMDAN-WT method, the signal is decomposed into different intrinsic mode functions (IMFs), and relevant parameters are selected to obtain IMF denoised signals through WT method for the noisy mode components with low sample entropy. The final pure signal is obtained by reconstructing the unprocessed mode components and the denoising component, effectively separating the signal from the wave interference.

Findings – The three methods of empirical mode decomposition (EMD), ensemble empirical mode decomposition (EEMD) and CEEMDAN are compared and analyzed by simulation. The simulation results show that the CEEMDAN method has higher signal-to-noise ratio and smaller reconstruction error than EMD and EEMD. The feasibility and practicability of the combined denoising method are verified by indoor and outdoor experiments, and the underwater acoustic experiment data after processing are combined beams. The problem of blurry left and right sides is solved, and the high precision orientation of the target is realized.

Originality/value – This algorithm provides a theoretical basis for MEMS hydrophones to achieve accurate target positioning in the ocean, and can be applied to the hardware design of sonobuoys, which is widely used in various underwater acoustic work.

Keywords MEMS vector hydrophone, CEEMDAN, Intrinsic mode function, Wavelet transform, DOA estimation

Paper type Research paper

1. Introduction

As an important acoustic sensor, hydrophones have a wide range of applications in the fields of marine resource exploration, underwater acoustic communication, data transmission, marine environment monitoring and underwater target recognition (Ferguson and Speechley, 2009). Scalar hydrophones need to be multiple for positioning, which leads to high cost and complex operation (Shang *et al.*, 2020; Yang *et al.*, 2021). The sound field has both sound pressure and vibration velocity, and the traditional vector hydrophone can estimate the azimuth angle of the target sound source according to this characteristic. The combination of microelectromechanical system (MEMS) processing technology and traditional underwater acoustic detection has promoted the development of miniaturization and low cost, and a number of MEMS hydrophones have emerged. Zhang *et al.* began to develop a piezoresistive MEMS vector hydrophone in 2004, with an operating frequency of 10 Hz–2 kHz and sensitivity of -170 dB@1 kHz (re 1 V/μPa). Compared with a scalar hydrophone, the MEMS vector hydrophone can pick up both scalar and vector information of the underwater acoustic field, and it has the characteristics of small-scale, low power consumption and high sensitivity. Single vector hydrophone can solve the problem of left and right side blur by combining beam and can realize direction of arrival (DOA) estimation of underwater acoustic target (Liu *et al.*, 2014; Zhang *et al.*, 2021; Zhang *et al.*, 2009; Zhu *et al.*, 2021). However, the complex and variable nature of the marine environment and the unnatural sound sources such as various ships and military sonar (Siddagangaiah *et al.*, 2016) pose great challenges to the signal acquisition and information transmission of the feedphone. Marine ambient noise interferes with the signal quality of feedphones and brings about a qualitative decline, and it has also brought great difficulties in accurate underwater target location (Wu *et al.*, 2024). Therefore, it is crucial to preprocess the

The current issue and full text archive of this journal is available on Emerald Insight at: **https://www.emerald.com/insight/0260-2288.htm**

Sensor Review
44/5 (2024) 545–562
© Emerald Publishing Limited [ISSN 0260-2288]
[DOI 10.1108/SR-04-2024-0293]

Ministry of Science and Technology of the People's Republic of China, National Natural Science Foundation of China (52175553, 61927807)

Received 3 April 2024
Revised 29 May 2024
Accepted 30 May 2024

original signal to remove noise (Jia et al., 2023; Shang et al., 2023; Wu et al., 2023).

To denoise the ambient noise in the ocean, many scholars have proposed many denoising methods (Du et al., 2017; Gao et al., 2017). The traditional signal denoising methods are finite impulse response (FIR) filters (Johansson, 2012) and infinite impulse response (IIR) filters (Al-Alaoui, 2007). However, such methods tend to cause group delay and phase distortion and have poor denoising performance. Compared with these traditional algorithms, EMD is more suitable for nonlinear and nonstationary signals (Qu et al., 2014). EMD is a novel adaptive signal time–frequency processing method creatively proposed by N. E. Huang and others in NASA in 1998. It is a completely adaptive decomposition method, which overcomes the limitations of standard time–frequency analysis by decomposing signals into multiple intrinsic mode functions (IMF) adaptively. However, the distribution of mode aliasing interference in time domain and frequency domain is also a problem (Li et al., 2018). To solve this problem, in 2009, Norden E. Huang and other scientists proposed integrated empirical mode decomposition (EEMD). Although it can effectively solve the mode aliasing problem, additional noise is not completely eliminated in the decomposition process, resulting in increased reconstruction errors (Luo et al., 2022). The CEEMDAN method, which was first proposed by Torres et al in 2009, is a further improvement of the EEMD algorithm. Generally, the components with more noise in the decomposed IMF components are determined according to different criteria, and the IMF components with more noise are eliminated for denoising. This leads to a lack of effective information (Colominas et al., 2014; Hu et al., 2023; Luo et al., 2023). The wavelet threshold (WT) denoising method, proposed by Donoho, is essentially to suppress the useless part of the signal and enhance the useful part, but it is easy to ignore the effective signal with a small threshold value, resulting in the loss of weak signals (Cai, 2019).

In response to different denoising methods, this paper proposes an algorithm based on CEEMDAN and WT joint denoising. The algorithm first decomposes the raw signal received by the MEMS vector hydrophone into a series of intrinsic mode components, then uses relevant parameters to filter and process the noisy intrinsic mode components with small sample entropy using wavelet thresholding to obtain the IMF denoising signal. Next, the untreated mode components are reconstructed with the denoised components to obtain the final clean signal. This processing method effectively removes noise while preserving useful features in the signal. Through indoor and outdoor experiments under natural conditions, the effectiveness and superiority of the algorithm have been verified. The algorithm successfully removes baseline drift and ocean noise and achieves high-precision orientation of the target during DOA estimation. It outperforms the literature (Hu et al., 2019; Jiang et al., 2024), is consistent with actual measurement conditions and the proposal of this joint algorithm is of great research significance for accurately locating underwater targets.

2. Algorithm part

2.1 EMD and EEMD

EMD is a data-driven time domain decomposition algorithm, which can adaptively decompose arbitrary signals into several basic mode components according to frequency and amplitude. The basic mode component (IMF) is a class of functions that meet the following two conditions. In the entire signal sequence, the number of extreme points (maximum and minimum points) and the number of zeros must be equal or at most not more than one difference. At any time, the average value of the upper envelope formed by the local maximum point and the average value of the lower envelope formed by the local minimum point is zero. The basic mode component that meets the above two conditions has only one extreme point between two consecutive zero crossings, that is, only one basic mode turbulence is enveloped and there is no complex superposition wave, which can reflect the inherent local volatility in the signal. The algorithm is a screening process. The basic flow of the algorithm is described as follows:

- Find all local extreme points on $x(t)$, connect all maximum points and all minimum points with a curve and obtain the upper envelope $f_{max}(t)$ and the lower envelope $f_{min}(t)$ of $x(t)$. Note the average value of $f_{max}(t)$ and $f_{min}(t)$ as $m(t)$.
- The difference between $x(t)$ and $m(t)$ is denoted as $h_1(t)$:

$$h1(t) = x(t) - m(t) \tag{1}$$

Ideally, $h_1(t)$ should be a fundamental mode component. However, because the signal is so complex, there may still be asymmetric waves in $h_1(t)$. Therefore, $h_1(t)$ is treated as the new $x(t)$, and the above operation is repeated until $h_1(t)$ is a basic pattern component, denoted as:

$$c1(t) = h1(t) \tag{2}$$

- After resolving the first basic mode component $c_1(t)$, subtract $c_1(t)$ from $x(t)$ to get the remaining signal:

$$x1(t) = x(t) - c1(t) \tag{3}$$

- Treat $x_1(t)$ as the new $x(t)$, repeat the above process and decompose successively to get:

$$\begin{cases} x_2(t) = x_1(t) - c_2(t) \\ x_3(t) = x_2(t) - c_3(t) \\ \vdots \\ x_n(t) = x_{n-1}(t) - c_n(t) \end{cases} \tag{4}$$

The stop criteria for the screening process are met, usually by limiting the size of the standard SD between two consecutive processing results $h_{1(k-1)}(t)$ and $h_{1k}(t)$:

$$SD = \sum_{t=0}^{T} \frac{\left|h_{1(k-1)}(t) - h_{1k}(t)\right|^2}{h_{1k}^2(t)} \tag{5}$$

where, T represents the time span of the signal.

The value of SD should be 0.2–0.3. The last remaining $x_n(t) = r_n(t)$ is the residual of the original signal.

In this way, through EMD decomposition, the signal $x(t)$ is decomposed into n fundamental components $c_i(t)$, $i = 1,2,\ldots$ The linear sum of n and a co-term $r_n(t)$:

Sensor Review
Volume 44 · Number 5 · 2024 · 545–562

$$x(t) = \sum_{i=1}^{n} ci(t) + rn(t) \tag{6}$$

From the above decomposition process, it can be seen that EMD starts by separating the basic mode component with the smallest feature time scale in the signal, then proceeds to separate the basic mode component with the larger feature time scale. Therefore, EMD can be regarded as a set of high-pass filters with signal adaptability.

When calculating the extreme envelope of the signal, EMD employs the cubic spline difference algorithm twice, resulting in envelope overshooting and undershooting. Additionally, after the signal is decomposed by EMD, some IMFs may contain multiple time-scale components, leading to mode aliasing. EEMD represents a significant improvement over the original EMD method by introducing small-amplitude white noise into the signal. This addresses the mode aliasing issue by equalizing the characteristics of the white noise spectrum.

The specific decomposition steps are as follows:

1 add a white noise sequence to the original signal;
2 the signal with added white noise is decomposed into a series of IMF by EMD algorithm;
3 repeat Steps 1 and 2, but add different white noise sequences each time; and
4 take the integrated average value corresponding to IMFs obtained each time as the final decomposition result.

2.2 CEEMDAN

The EEMD algorithm is to add Gaussian white noise or pairs of positive and negative Gaussian white noise to the decomposed signal to eliminate the mode aliasing problem of EMD decomposition. However, such algorithms do not isolate residual noise, resulting in the added white noise signal that can always be transferred from high frequency to low frequency. Therefore, there will always be some white noise signal left in the eigen-component of the decomposed mode, which will affect the subsequent signal analysis and processing. In 2011, Torres M.E *et al.* proposed a novel signal decomposition algorithm, CEMMDAN, which is a complete decomposition method and better solves the mode aliasing phenomenon existing in EEMD.

Let IMF_m be the *m-th* eigenmode component that is obtained after EMD decomposition, $V_i(t)$ be the Gaussian white noise signal satisfying the standard normal distribution, ε be the standard deviation of the noise and $x(t)$ be the original signal:

- Adding pairs of positive and negative Gaussian white noise to the original signal $x(t)$ gives a new signal $x(t)+(-1)^{p}\varepsilon v_i(t)$, where $p = 1$ or 2. After EMD decomposition of the new signal, N modal components are aggregated and averaged to obtain:

$$\overline{IMF1(t)} = \frac{1}{N}\sum_{\mathrm{i}=1}^{N} IMF_1^{\mathrm{i}}(t) \tag{7}$$

- Calculate the residual after removing the first modal component:

$$r1(t) = x(t) - \overline{IMF1(t)} \tag{8}$$

- A new signal is obtained by adding positive and negative pairs of Gaussian white noise to $r_1(t)$, and the first mode component D_1^j is obtained by EMD decomposition using the new signal as the carrier, and then the second mode component can be obtained:

$$\overline{IMF2(t)} = \frac{1}{N}\sum_{j=1}^{N} D_1^j(t) \tag{9}$$

- Calculate the residual by removing the second modal component:

$$r2(t) = r1(t) - \overline{IMF2(t)} \tag{10}$$

- Repeat the above steps until the obtained residual signal is a monotone function and cannot be decomposed further, and the algorithm ends. At this time, the number of eigenmode components obtained is K, then the original signal $x(t)$ is decomposed into:

$$x(t) = \sum_{k=1}^{K} \overline{IMFk(t)} + rk(t) \tag{11}$$

By the improved decomposition of CEEMDAN into multiple IMFs and residuals, the frequency of IMFs varies from high to low frequency.

2.3 IMF selection criteria

The CEEMDAN algorithm is primarily designed to remove noise from the dominant modal component of the signal and retain its main components, while the decomposed IMF components decrease the signal frequency with the increase in order. Not all of the decomposed IMF components can correctly express the effective features of signal $x(t)$, so the extraction of effective IMF is the key to reconstruct the signal. The correlation coefficient is used to determine the Q value of the indexing point, so that IMF_Q-IMF_N is the dominant signal modal component of the signal. Suppose the correlation coefficient between IMF_i and the original signal $x(t)$ is ρ, x is the original signal and y is the *I-order* IMF component. The better the correlation between the two, the more active components of $x(t)$ will be. The correlation coefficient is defined as follows:

$$\rho xy = \frac{\sum_{i=1}^{N}(xi-\overline{x})(yi-\overline{y})}{\sqrt{\sum_{i=1}^{N}(xi-\overline{x})}\sqrt{\sum_{i=1}^{N}(yi-\overline{y})}} \tag{12}$$

The absolute value of ρ is between 0 and 1, and in general, the closer ρ is to 1, the stronger the correlation between the two quantities x and y. In addition, sample entropy is introduced to describe the regularity and complexity of the sample data and measure the correlation between the data. White noise is independent of each other and there is no correlation, while data signals contain regular sinusoidal pulses with stable correlation. Therefore, sample entropy can be used to determine the

Sensor Review
Volume 44 · Number 5 · 2024 · 545–562

correlation scale between IMF component and the original signal. The more complex and irregular the data, the larger the sample entropy; on the contrary, the higher the self-correlation of the data, the smaller the sample entropy.

2.4 Wavelet threshold denoising algorithm

The WT denoising method was proposed by Donoho in 1995. The wavelet transform decomposes the signal through translation and scaling operations, which is equivalent to passing the signal through a set of bandpass filters with different bandwidths and center frequencies. Due to the complexity and variability of the underwater acoustic environment, the target signal is generally a low frequency and relatively stable signal, while the noise is mostly a high frequency or pulse intermittent signal.

Choosing the appropriate threshold function to denoise the signal is the key index to measure the performance of the algorithm.

Definition of hard threshold function:

$$\eta(x,\lambda) = \begin{cases} x & |x| \geq \lambda \\ 0 & |x| < \lambda \end{cases} \tag{13}$$

Definition of soft threshold function:

$$\eta(x,\lambda) = \begin{cases} \operatorname{sgn}(x)(|x|-\lambda) & |x| \geq \lambda \\ 0 & |x| < \lambda \end{cases} \tag{14}$$

x is the wavelet coefficient, λ is the threshold and *sgn(x)* is the symbolic function, and its expression is:

$$\operatorname{sgn}(x) = \begin{cases} 1 & x > 0 \\ 0 & x = 0 \\ -1 & x < 0 \end{cases} \tag{15}$$

The hard threshold function retains wavelet coefficients higher than the set threshold and sets the wavelet coefficients lower than the threshold value in each space to 0. The soft threshold function shrinks the wavelet coefficients according to the set fixed amount, and then reconstructs the denoised signals from the new wavelet coefficients. The signals denoised by the soft threshold value have better smoothness and continuity. Therefore, this paper selects the soft threshold function to denoise the signal received by the vector hydrophone.

On the basis of the above theory, a processing method for nonstationary signals can be proposed: the signal was decomposed by CEEMDAN, and the correlation coefficients between each IMF component and the original signal are calculated. The IMF component with low sample entropy is denoised by wavelet soft thresholding, and the denoised IMF component and the nondenoised IMF component are reconstructed by selecting appropriate decomposition layers to obtain the denoised signal *X' (t)* after the joint denoising method.

To further highlight the effectiveness and superiority of the combined CEEMDAN-WT algorithm proposed in this paper in the pre-processing of underwater acoustic signals, the signal-to-noise ratio (SNR) and the root mean square error (RMSE) are used as performance indicators to evaluate the signals collected by vector hydrophones. The higher the SNR and the lower the root-mean-square error, the better the denoising effect and the more complete the effective signal components are preserved. The SNR and RMSE error are calculated as follows: *X(i)* is the original pure signal, *X' (t)* is the denoised signal and n is the signal length:

$$SNR = 10 \times \lg\left(\frac{\sum_{i=1}^{n} X'(i)^2}{\sum_{i=1}^{n}\left(X(i)^2 - X'(i)^2\right)}\right) \tag{16}$$

$$RMSE = \sqrt{\frac{1}{n}\sum_{i=1}^{n}\left(X(i) - X'(i)\right)^2} \tag{17}$$

2.5 Sound pressure–vibration velocity processing algorithm

Through the above improved CEEMDAN-WT joint denoising algorithm, the data are pre-processed to achieve the effect of denoising and correcting the baseline drift, and the processed signal *X' (t)* is combined into a beam to solve the problem of fuzzy left and right sides and achieve the accurate orientation of the target. The combined beam theory is as follows (Zhu *et al.*, 2022).

For a single vector sensor, the sound pressure hydrophone is nondirectional, and the vibration velocity sensor is even sub-directional, as shown in Figure 1. A vector sensor combining sound pressure and vibration velocity outputs the orthogonal three-dimensional vibration velocity component of sound pressure at the same point. Figure 2 shows the projection diagram of vibration velocity V and its three orthogonal components v_x, v_y and v_z. Assume that the sound source position is S, the hydrophone position is O, θ is the horizontal azimuth, the positive x-axis corresponds to 0°, α is the elevation angle and the horizontal plane *(xOy)* is at 0°.

The model of vector hydrophone picking up signal can be expressed as:

In the ocean waveguide, the vertical direction exhibits a standing wave pattern, so only the two-dimensional directivity of the horizontal direction is considered:

$$\begin{cases} p(t) = x(t) \\ v_x(t) = x(t)\cos\theta \\ v_y(t) = x(t)\sin\theta \end{cases} \tag{18}$$

where, $x(t)$ is the target sound pressure signal, $p(t)$ is the sound pressure signal picked up by the vector hydrophone and $v_x(t)$ is the vibration velocity signal of x axis picked up by the vector hydrophone. $v_y(t)$ is the vibration velocity signal of y axis picked up by the vector hydrophone.

In formula equation (18), two orthogonal vibration velocity components v_x and v_y are combined, and the combined vibration velocity v_c and v_s are obtained:

$$\begin{cases} v_c(t) = v_x(t)\cos(\psi) + v_y(t)\sin(\psi) \\ v_s(t) = -v_x(t)\sin(\psi) + v_y(t)\cos(\psi) \end{cases} \tag{19}$$

where ψ is the guiding azimuth in equation (19); bringing equation (18) into equation (19), we obtain:

$$\begin{cases} v_c(t) = x(t)\cos(\theta - \psi) \\ v_s(t) = x(t)\sin(\theta - \psi) \end{cases} \tag{20}$$

Figure 1 Directional diagram of sound pressure and vibration velocity

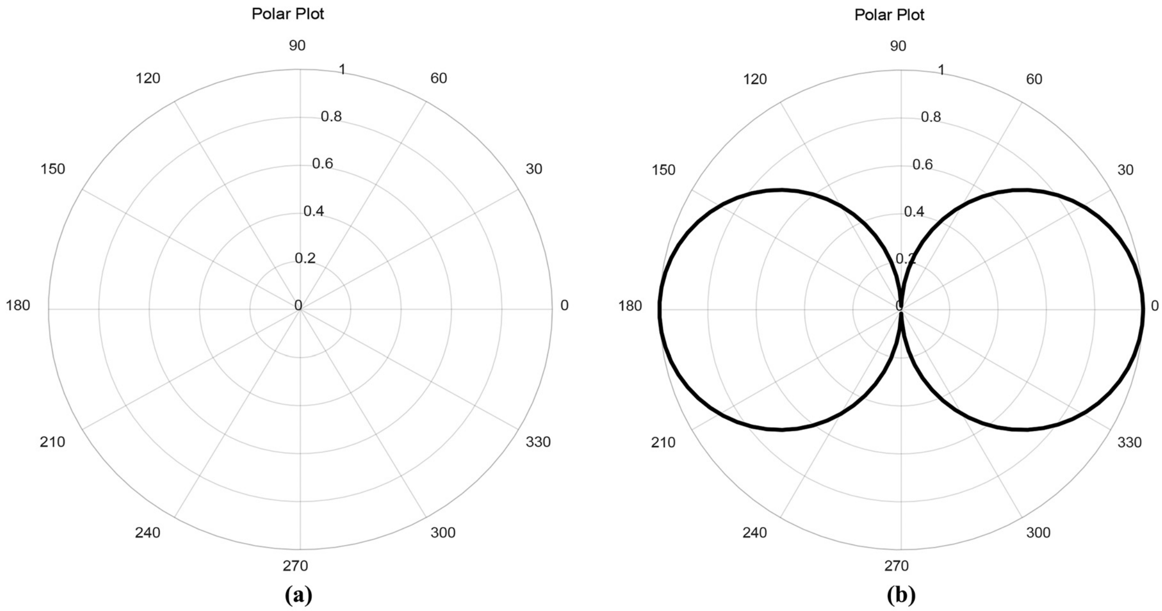

Notes: (a) Directional map of sound pressure; (b) directional diagram of vibration velocity
Source: Created by authors

Figure 2 Projection of vibration velocity V and its three orthogonal components V_x, V_y and V_z

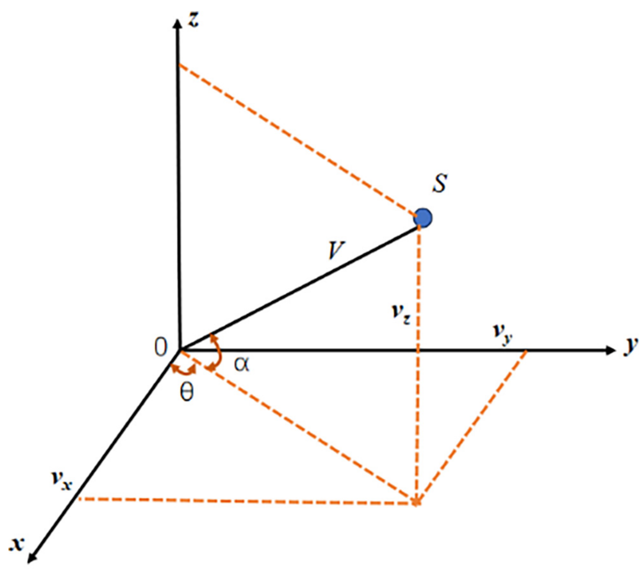

Source: Created by authors

In formula equation (20), v_c and v_s still represent orthogonal dipole directivity. The guiding azimuth ψ corresponds to the principal maximum direction of v_c and the directional zero direction of vs. This denotes the relative azimuth between the target sound source and the hydrophone.

In Figure 1(b), the directivity of vibration velocity in the middle has the feature of "8" font, which leads to the estimated azimuth containing two fuzzy angles with a difference of 180°, and the true direction of the target cannot be uniquely determined.

In this paper, sound pressure $p(t)$ and vibration velocities $v_x(t)$ and $v_y(t)$ are weighted and combined to form a unilateral directional form, as shown in Figure 3:

$$[p(t) + v_c(t)]^2 = x^2(t)[1 + \cos(\theta - \psi)]^2 \tag{21}$$

Its corresponding directivity is as follows:

$$R(\theta) = \cos^4 \frac{\theta - \psi}{2} \tag{22}$$

3. Simulation and comparison

3.1 Simulated signal

There are many types of noise in the marine environment, and they are distributed in different frequency bands. To ensure that the signal can be transmitted over long distances, we need to place it in the low frequency range. Therefore, for signals with strong noise, denoising and correction analysis of baseline drift become very important. To verify the feasibility of the CEEMDAN-WT method introduced in this paper without losing its general nature, the simulation signal is first denoised. We assume that the signal $x(t)$ received by the vector hydrophone consists of target signal $s_0(t)$, baseline drift signal $BL(t)$ and Gaussian white noise $n(t)$:

$$x(t) = s0(t) + n(t) + BL(t) \tag{23}$$

where, $s_0(t)$ is the original signal, $n(t)$ is white Gaussian noise and $BL(t)$ is the baseline.

The sampling frequency is 1,000, that is to say, the analog signal is sampled 1,000 times/s. The most basic sinusoidal

Figure 3 Combination directivity

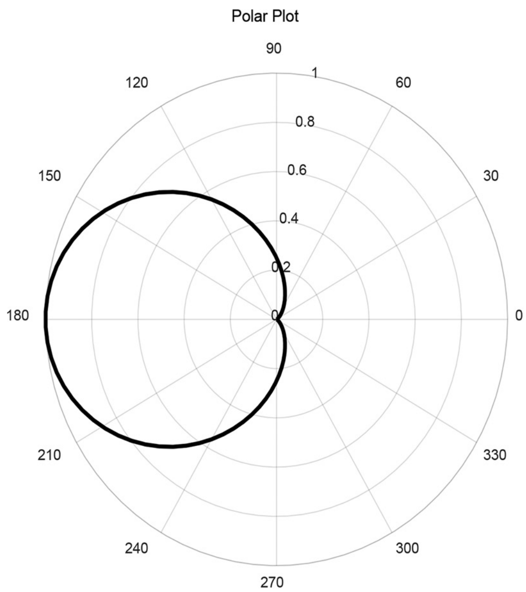

(a)

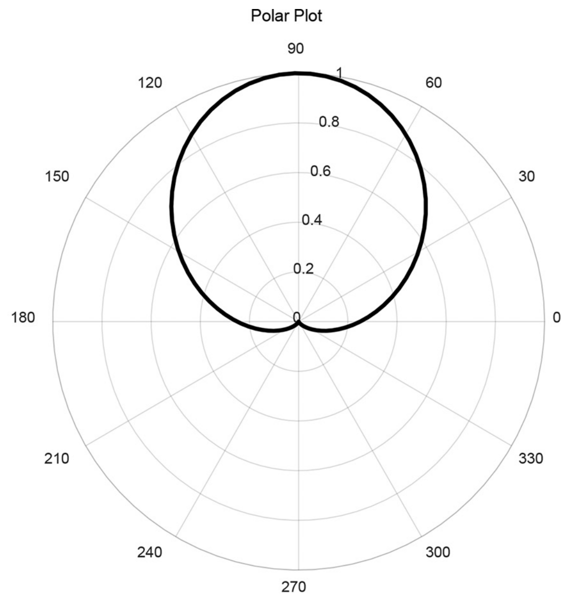

(b)

Notes: (a, b) The directivity of $(p + v_c)^2$
Source: Created by authors

signal, The angular frequency is 20, is replaced with a sinusoidal signal of only three cycles, and 0.5 mean Gaussian white noise is added to the whole time domain, and finally a continuous DC 1 is added as the baseline for its drift. The constructed signal is shown in Figure 4.

3.2 Signal decomposition and comparison

When decomposing the simulation signal using EMD, EEMD and CEEMDAN algorithms, we set the standard deviation of additional noise to 0.2, with a signal-to-noise ratio of 0 dB and a set size of 500, to avoid excessive noise affecting the signal decomposition. In Figures 5–7, it can be observed that significant mode aliasing exists among the basic mode components in the EMD method, while the degree of mode aliasing in EEMD and CEEMDAN methods is noticeably reduced. Additionally, to obtain data for each eigenmode component, it is crucial to determine the signal and noise components to prepare for subsequent wavelet denoising and signal reconstruction. Taking each IMFs obtained from CEEMDAN decomposition in Figure 7 as an example, we calculate the correlation between each modal component and the original signal using the concept of correlation coefficient in MATLAB. Based on the absolute value of correlation, we can screen the effective signal components with noise that need to be processed.

Figure 4 Signals containing baseline drift and Gaussian white noise

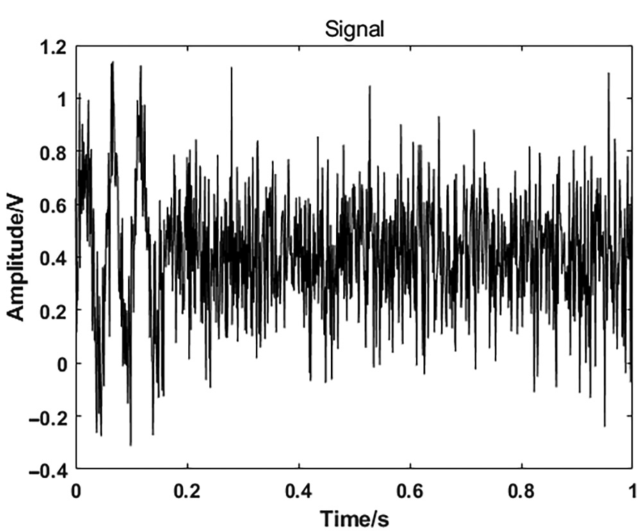

Source: Created by authors

Table 1 displays all correlation coefficients between IMFs and the original signal. By comparing the coefficients of different intrinsic modal components with the original signal, modes with correlation coefficients close to 1 are retained. It is inferred that the correlation coefficients of IMF_3–IMF_6 are above 0.2, indicating strong correlation with the original signal, and thus considered dominant mode components, while the correlation between IMF_1–IMF_2 and IMF_7–IMF_9 and the signal is weak. Additionally, the same conclusion can be drawn from the waveform comparison in Figure 7.

Additionally, we can utilize sample entropy quantization to screen appropriate intrinsic modal components. Sample entropy serves as a quantitative measure of signal complexity, enabling us to assess its characteristics based on the decomposed intrinsic modal components and the signal's sample entropy. A smaller sample entropy indicates lower time series complexity, higher self-similarity and

Figure 5 EMD result

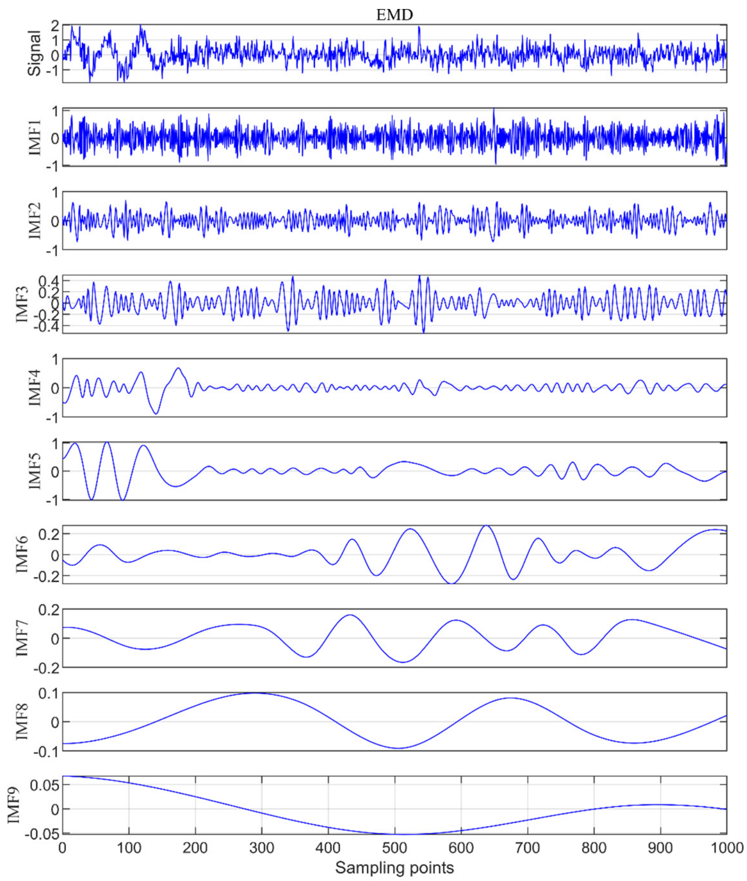

Source: Created by authors

greater correlation with the signal; conversely, a larger sample entropy suggests lower time series autocorrelation. The improvement over reference (Hu *et al.*, 2019; Jiang *et al.*, 2024) lies in the easier selection of effective intrinsic mode functions, thereby better distinguishing signals from noise.

As seen in Table 2, the sample entropy of IMF_3–IMF_6 is small, indicating that these modal components contain more effective components of the original signal. The intrinsic modal components containing noise are subjected to wavelet thresholding, and the wavelet parameters in the wavelet thresholding denoising process are set to: sym12 (good and simple denoising), HeurSure thresholding, soft thresholding function, and the decomposition level is 5. Figures 8–10 display the pure signal reconstructed after denoising the modal components with wavelet thresholding and the unprocessed modal components. The original signal and the reconstructed signal are depicted in different colors. From the figures, it's evident that these three methods can eliminate existing noise components while maintaining local waveform characteristics and peak values, thus restoring the signal with a certain accuracy. Comparatively, the signal reconstructed by the CEEMDAN method retains more complete and smoother effective signal components, superior to the literature (Jiang *et al.*, 2024); it is able to fully recover the waveform in the time domain, followed by the EEMD method, whereas the signal reconstructed by the EMD method contains some sharp peaks.

To further highlight the advantages of the CEEMDAN combined WT denoising method proposed in this paper, −8-8 dB white Gaussian noise is added to the original signal, and the signal-to-noise ratio and root-mean-square error of the denoising signal processed by the three methods are calculated as evaluation indicators to analyze the denoising effect of different denoising methods. Figures 11–12 shows the result.

According to the denoising evaluation criteria, comparing the denoising evaluation indicators in Figures 11–12, it can be seen that the output signal-to-noise ratio of the CEEMDAN combined wavelet denoising method is higher than the other two methods, and the white noise removal effect is better. Meanwhile, with the increase of the signal-to-noise ratio, the root-mean-square error gradually increases, indicating that this denoising method is feasible under both low and high noise thresholds.

To reflect the short calculation time of CEEMDAN decomposition, which is convenient for hardware implementation and has great advantages in engineering application, the total number of iterations of EEMD and CEEMDAN decomposition methods is calculated. Under this signal, the total number of iterations of EEMD and CEEMDAN is 7,649, and the total number of iterations of

Sensor Review
Volume 44 · Number 5 · 2024 · 545–562

Figure 6 EEMD result

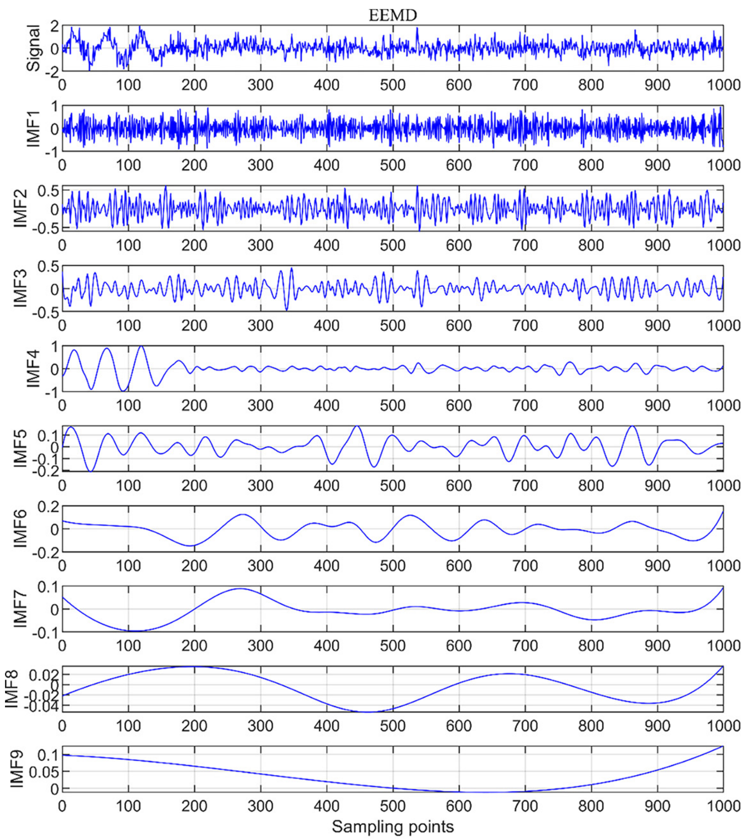

Source: Created by authors

CEEMDAN is 2,516. This method provides an improvement in computational cost, requiring only 32.9% EEMD screening iterations for the signal.

4. Results and discussion

4.1 Performance calibration of MEMS vector hydrophone

The ciliary vector hydrophone based on the bionic principle independently developed by North University of China contains two vector channels and one sound pressure channel (Geng *et al.*, 2023). MEMS hydrophones must be calibrated for sensing performance to be used as standard measuring equipment. The current calibration method for low-frequency underwater acoustic sensors at home and abroad is the standing wave field calibration method. At the bottom of the standing wave tube is an emission transducer, which can be viewed as a vertical sound transmission circular tube with an absolutely hard tube wall, where the sound pressure at the water–air interface is zero. Figures 13–14 shows the test principles and test site. The test instruments mainly include standing wave tube, MEMS vector hydrophone, scalar hydrophone, vertical coordinate rotation device, control instrument, programmable electronic switch, signal generator and digital oscilloscope, programmable filter, preamplifier, DC stable source, power amplifier and test software, and the experiment process is marked with red arrows. In Figure 14, the vector sensor under test is enlarged in the red box. For MEMS vector hydrophones used in indoor and outdoor experiments, the sensitivity of X, Y and p channels at 1 kHz is -180.2 dB, -180.8 dB and -180.5 dB (0 dBre 1 V/μPa), respectively, and the maximum error of vector channels is less than 0.5 dB, as shown in Figure 15. Figure 16(a) shows the directivity diagram of the vector hydrophone, the X and Y channels are figure 8-shaped, the directional resolution of the hydrophone is greater than 30 dB, the symmetry and consistency of the two vectors are good and the depth of the concave points are 47.6 dB and 43.6 dB, respectively. The directivity of sound pressure channel is omnidirectional. The MEMS hydrophone has good performance and can meet the requirements of indoor and outdoor experiments.

4.2 Experimental verification in indoor environment

To evaluate and verify the effectiveness of this algorithm, the "8" character directivity of MEMS vector hydrophone was tested in an indoor anechoic pool with a length, width and height of 9.6 × 6 × 6 m. The test and experiment site are shown in Figure 17. The red block diagram on the left is the acquisition data system NI PXIE-6358, and the red block diagram on the right is the launch data system: the fish-lip transducer and the signal generator, the middle block diagram is an anechoic pool in an indoor environment, the movable slide rail is installed and the platform is movable,

Sensor Review
Volume 44 · Number 5 · 2024 · 545–562

Figure 7 CEEMDAN result

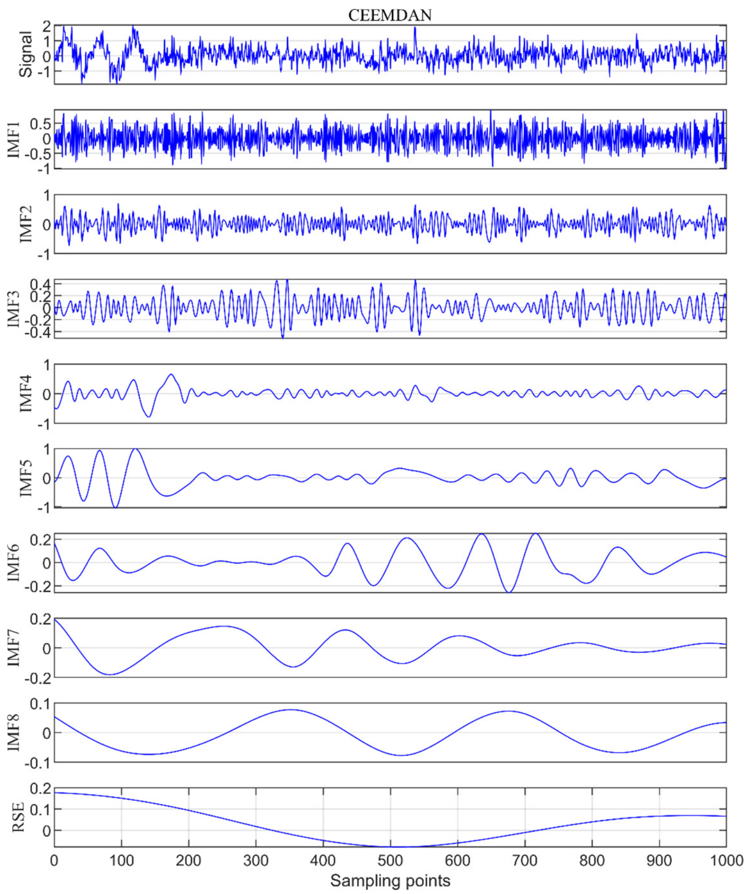

Source: Created by authors

Table 1 IMF correlation coefficient

IMF_i	IMF_1	IMF_2	IMF_3	IMF_4	IMF_5	MF_6	IMF_7	IMF_8	IMF_9
ρ_i	0.1260	0.1059	0.2531	0.2417	0.4614	0.2600	0.0680	0.0649	0.0532

Source: Created by authors

Table 2 Sample entropy of IMF

IMF_i	IMF_1	IMF_2	IMF_3	IMF_4	IMF_5	MF_6	IMF_7	IMF_8	IMF_9
SE	1.6117	1.9807	0.5046	0.4967	0.2337	0.3909	0.0861	0.0437	0.0213

Source: Created by authors

which can change the distance between the MEMS vector hydrophone and the sound device. The platform has a rotating device, an elastic fixed hydrophone and the operating device can change the rotation angle of the hydrophone.

The specific process of collecting experimental data is as follows: the MEMS hydrophone is fixed on the mobile platform by elastic suspension, and the hydrophone is rotated one turn by manipulating the platform rotation button. The fish-lip sensor and the MEMS vector hydrophone are placed together 3 m underwater, 9 m apart horizontally. Start the hydrophone power supply, use the signal generator to emit a sinusoidal pulse signal with a fixed amplitude (2 V) and a fixed frequency (315 Hz) within 1 s, and after being amplified by the power amplifier, the signal is transmitted to the fish-lip transducer in the anechoic pool, and the fish-lip transducer converts the electrical signal into an acoustic signal. The MEMS vector hydrophone converts the received acoustic signal into an electrical signal and amplifies it with an amplifier. Finally, the amplified signal is transmitted to the NI collection interface, and the laboratory data collection is completed.

Figure 8 EMD reconstruction signal

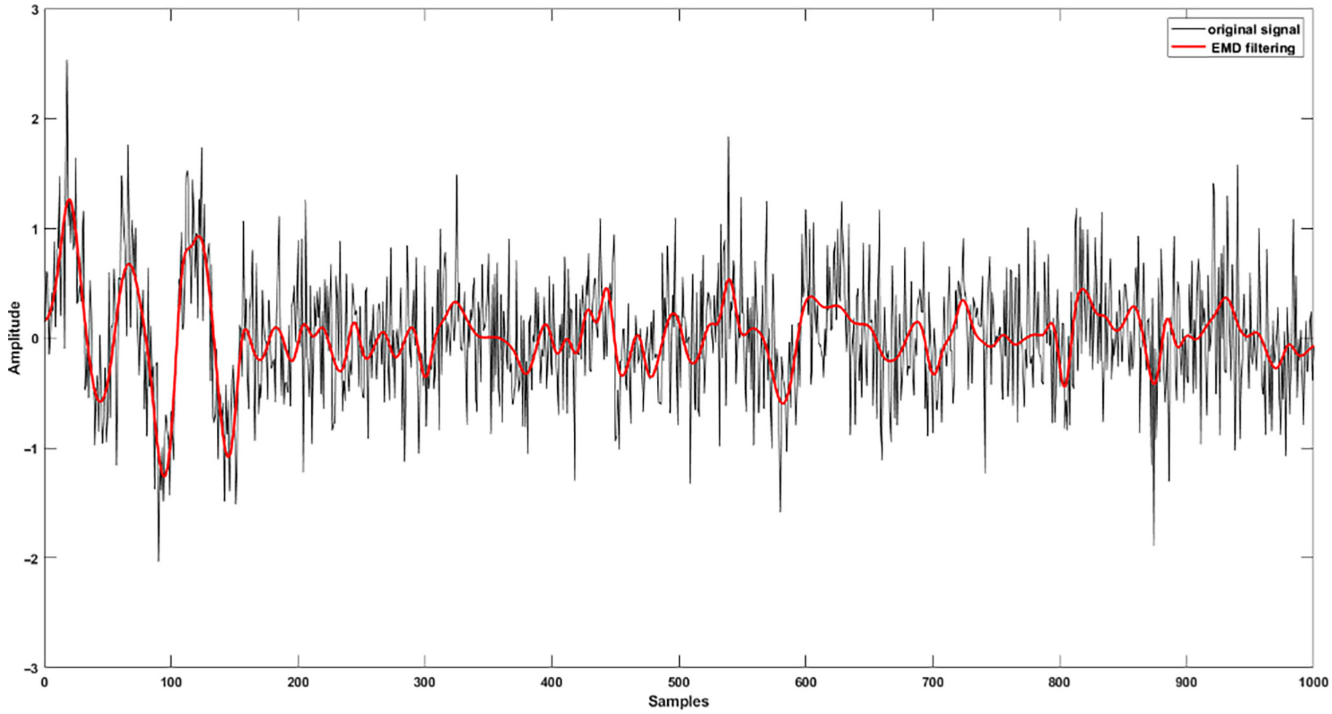

Source: Created by authors

Figure 9 EEMD reconstruction signal

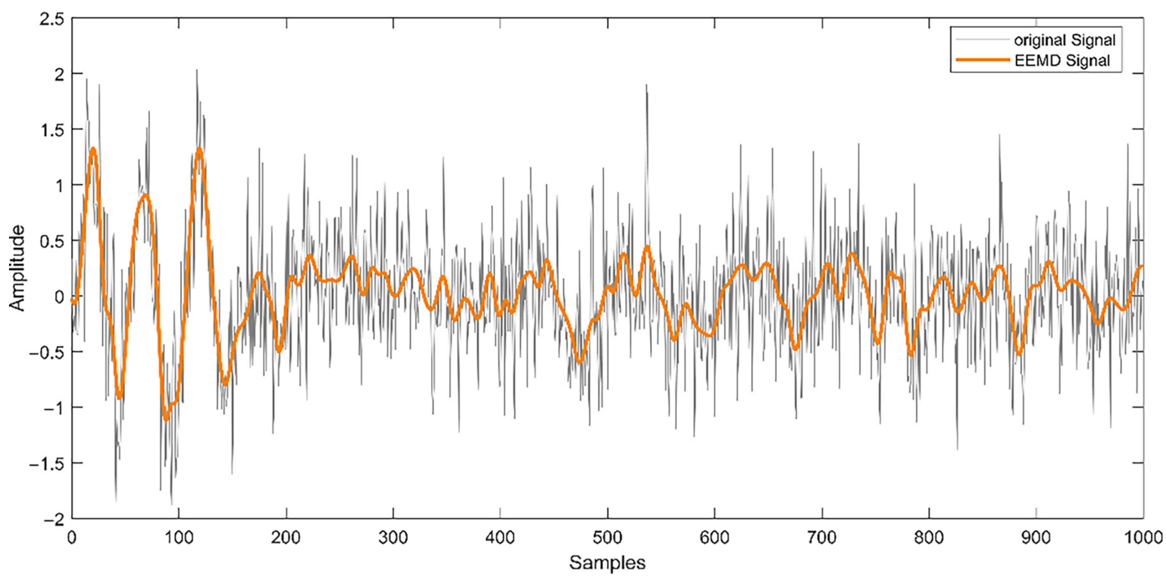

Source: Created by authors

Analysis of experimental results: Figure 18 shows the signal time domain diagram after CEEMDAN-WT processing, and the amplified signal time domain diagram is in the upper left box. The amplitudes of X and Y signals are orthogonal to each other in a rotation period, and the P-signal is omnidirectional. The results show that the CEEMDAN-WT method proposed in this paper can effectively restore the signal and realize the accurate acquisition of the sound source signal. The algorithm will be further verified in the outdoor environment for the accurate location of the sound source by combining the combined beam.

Figure 10 CEEMDAN reconstruction signal

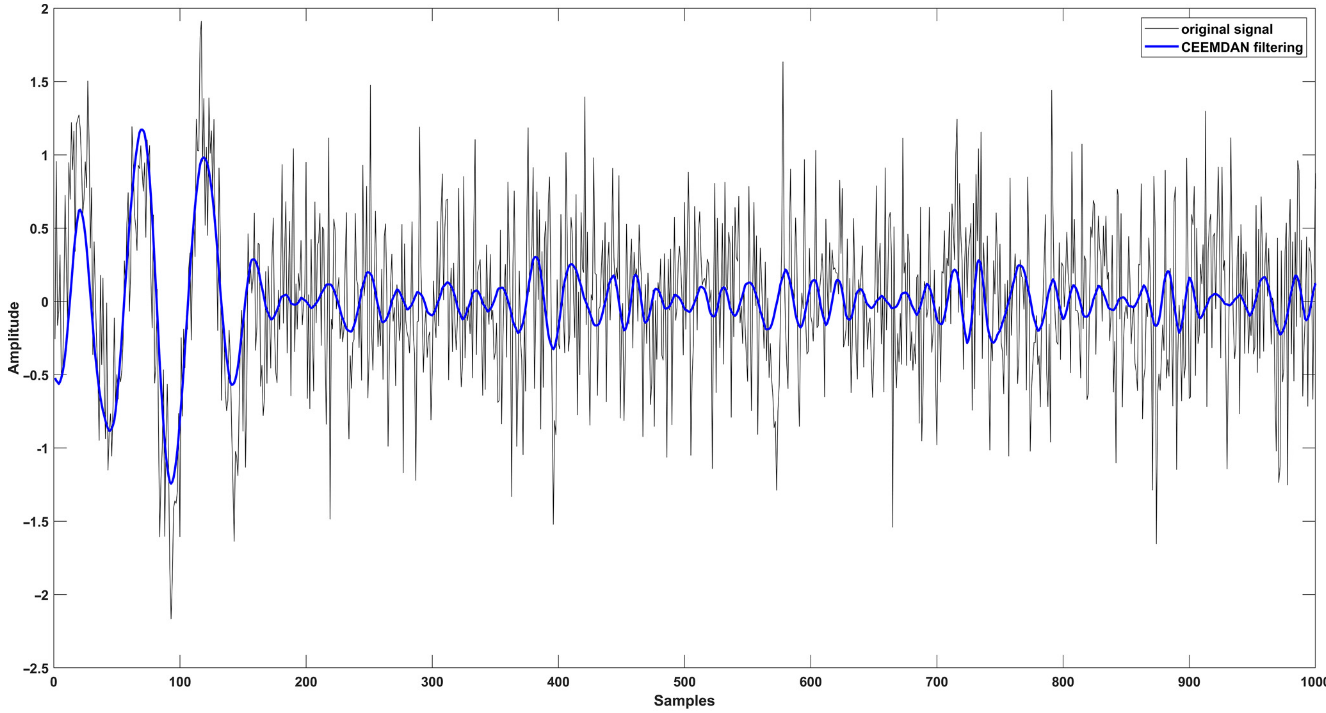

Source: Created by authors

Figure 11 Bar chart of signal-to-noise ratio changes of the three methods

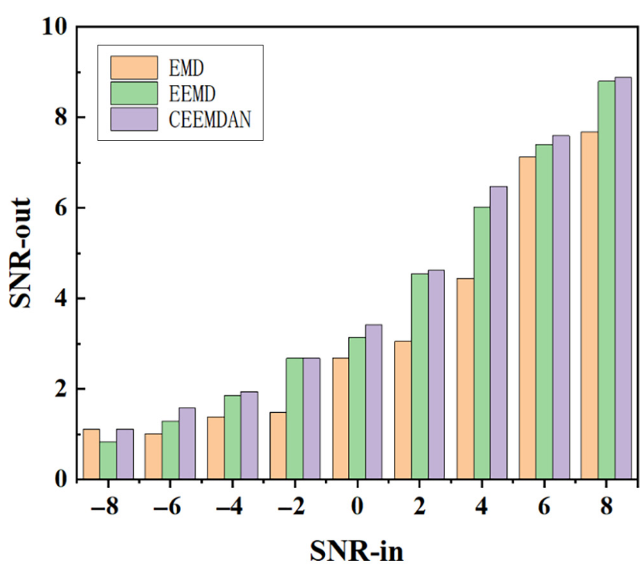

Source: Created by authors

Figure 12 Bar chart of RMS error changes of the three methods

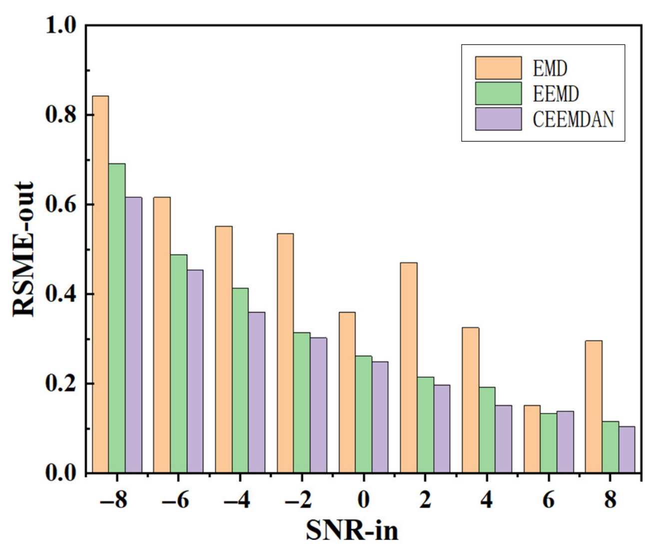

Source: Created by authors

4.3 Experimental verification in outdoor environment

To analyze the effectiveness and advantages of using this algorithm in the actual natural environment, an outfield experiment was conducted in the second reservoir of Fen He River, Taiyuan City, Shanxi Province. The experimental area is relatively open, with an average water depth of about 40 m and an open area of about 1 km^2. The working water depth and signal type are controllable, basically meeting the requirements of far-field conditions, and there is no interference from noise sources such as operating vessels on the water. The platform has strong stability and operability, so it can be regarded as an ideal test environment. The geometric placement diagram of the experimental data acquisition equipment is shown in Figure 19. The test equipment includes MEMS vector

Figure 13 Flow chart of hydrophone calibration system

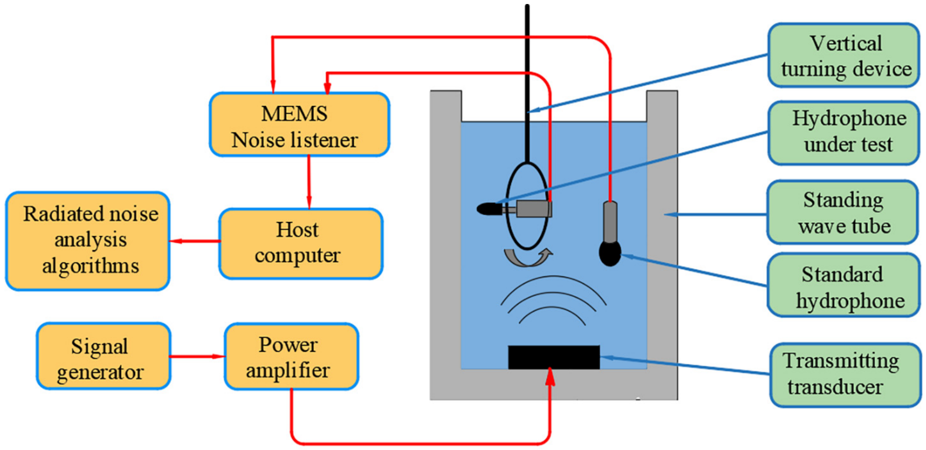

Source: Created by authors

Figure 14 Standing wave tube calibration field diagram

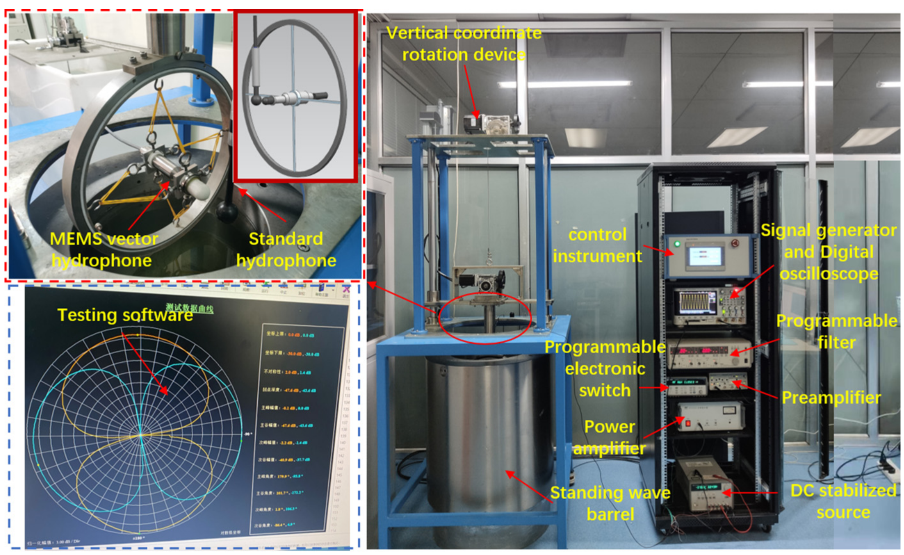

Source: Created by authors

hydrophone, standard sound transducer, mobile power supply, signal generator, index board, power amplifier, upper computer and NI PXLE-6358 data acquisition card.

The MEMS vector hydrophone and the sound source transceiver were placed on the ship. The experiment was divided into two groups. First, the support was designed and a single MEMS vector hydrophone was elastic fixed on it. The attitude information of the vector hydrophone is monitored and recorded in real time by the electromagnetic compass, where the north direction of the electromagnetic compass is parallel to the positive *x* direction of the MEMS vector hydrophone. Such a device can estimate DOA and calibrate the attitude of the hydrophone at the same time. Second, the standard sound transducer (operating frequency band 100–2,000 Hz) and the support for fixing a single MEMS hydrophone are placed 10 m underwater, and the index plate is connected to the other end of the support to determine the rotation angle of the hydrophone underwater. The horizontal distance between the hydrophone and the standard acoustic transducer is 50 m. The signal generator transmits a single-frequency signal, the signal frequency is 315 Hz, the peak-to-peak value is 1 V pulse signal, the pulse period is 1 s and the pulse width is three sinusoidal cycles (the signal-to-noise ratio is 13.52 dB). Finally, the received signal data will be recorded by the computer and NI PXLE6358 data acquisition card, and subsequent data analysis will be carried out. The experiment site diagram is shown in Figure 20.

In the first group, rotate the dial to change the position of the hydrophone relative to the sound source, the geodetic coordinate system with the vector hydrophone as the coordinate origin, due north as the *x*-axis forward, and due west as the *y*-axis forward, the angles of the four groups of position

Figure 15 Sensitivity of three channels

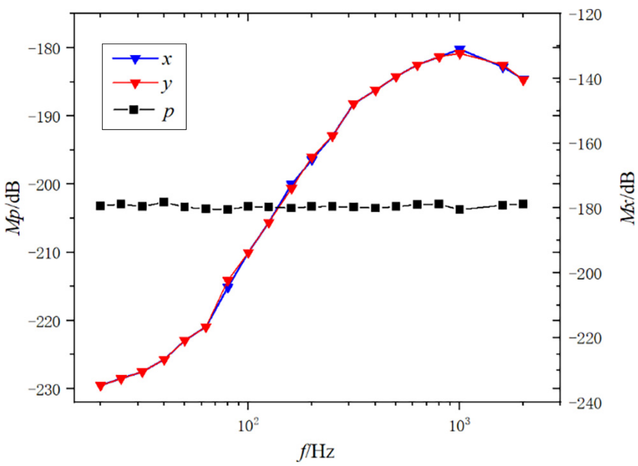

Source: Created by authors

sound sources relative to the hydrophone were obtained as [31.51°, 76.06°, 141.21°, 222.39°], which was used as the calibration basis for the calculation results. In the second group, use the index plate to manually rotate the vector hydrophone one circle, use the timer to record the rotation time of one circle for 3 min and collect three-way signals. Calculate the relative angle between the sound source and the hydrophone at different times.

Analysis of experimental results: The first group, taking the X-channel signal as an example, Figures 21 and 22 are the comparison of the effect in time domain and frequency domain of the original signal after CEEMDAN and CEEMDAN-WT processing, respectively. It can be seen that the signal clutter removal after CEEMDAN-WT processing is more thorough, and most of the noise and baseline drift problems are solved. Figure 23 shows the azimuth estimation results processed by the combined algorithm after denoising, which are presented in the weight statistical graph of normalized weighted probability. The horizontal coordinate corresponding to the maximum peak value of weighted probability 1 is the target azimuth angle, which is [31°, 78°, 141°, 222°]. There is no ambiguity regarding left and right sides; the orientation accuracy can reach 1°, and the maximum error is within 3°. The accuracy is better than that in the literature (Zhu *et al.*, 2022), and the direction error is less than 5°. The second set, Figure 24, is the pulse signal azimuth history diagram; (a) and (c) generate a 3D surface diagram, representing the distribution of data over time and angle. Figures 24(b) and 24(d), are the comparison of the combined orientation of the signal before and after CEEMDAN-WT filtering, respectively. It can be seen that the filtered signal can recover the effective original signal and obtain the angle change, and the azimuth angle increases from 27° to 357° and then from 3° to 32°. Within 180 s, the azimuth angle changed by 359°, the ballistic trajectory was clearly visible and it clearly showed that the hydrophone rotated once. The calculated results were consistent with the test conditions. Obviously 357° and 3° are the same position point on the vector hydrophone, so there will be a jump in the azimuth history chart. The test results show that the outdoor orientation error is less than 3°, and the method is still feasible in the complex ocean noise environment.

Figure 16 Three-way directional diagram

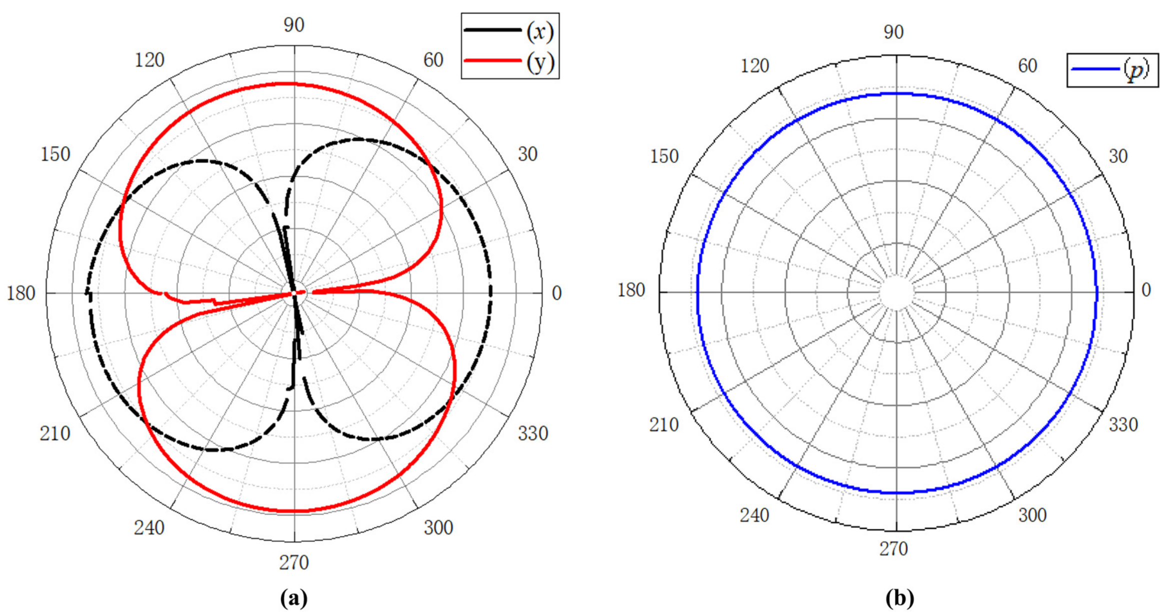

Notes: (a) Directional diagram of vector channel; (b) directivity diagram of scalar channel
Source: Created by authors

Figure 17 Laboratory test site diagram

Source: Created by authors

Figure 18 Time domain diagram of pulse signal

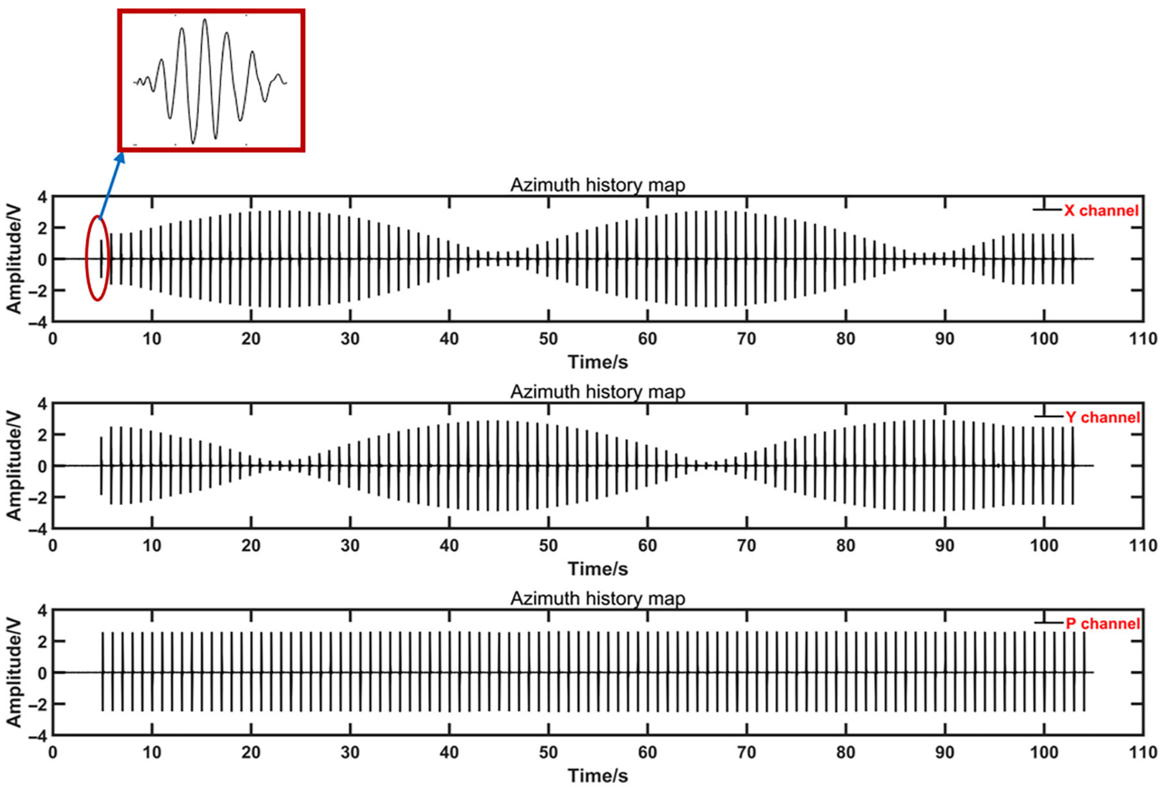

Source: Created by authors

5. Conclusion

In this paper, a new denoising and orientation method of single-vector MEMS hydrophone based on improved CEEMDAN-WT and combined beam combining is proposed. Through simulation, EMD and EEMD algorithms are discussed and compared in this study. This new denoising method utilizes the correlation coefficient method to select appropriate IMF components. For mode classification with small sample entropy, the high-frequency component containing noise is recovered using WT denoising, while retaining the original signal characteristics, thereby achieving better denoising effects. Moreover, by conducting experiments

Figure 19 Experimental diagram

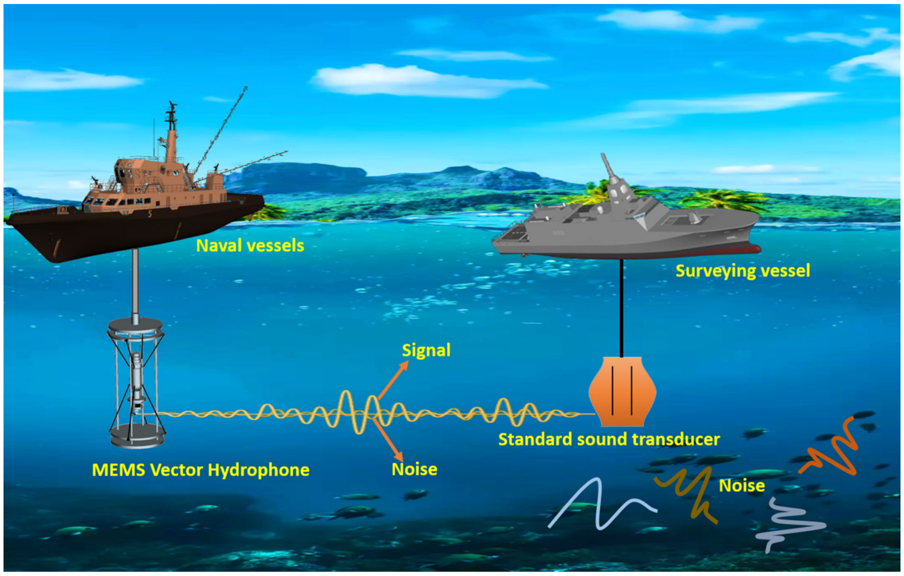

Source: Created by authors

Figure 20 Outdoor site drawing

Source: Created by authors

Figure 21 Based on CEEMDAN time domain and spectrum after denoising

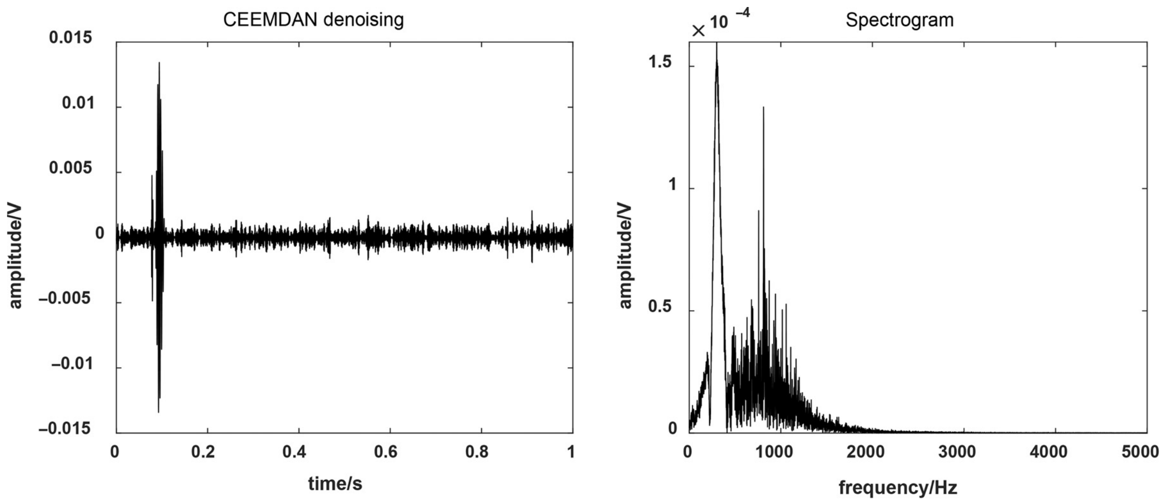

Source: Created by authors

Figure 22 Combined denoising signal and spectrogram

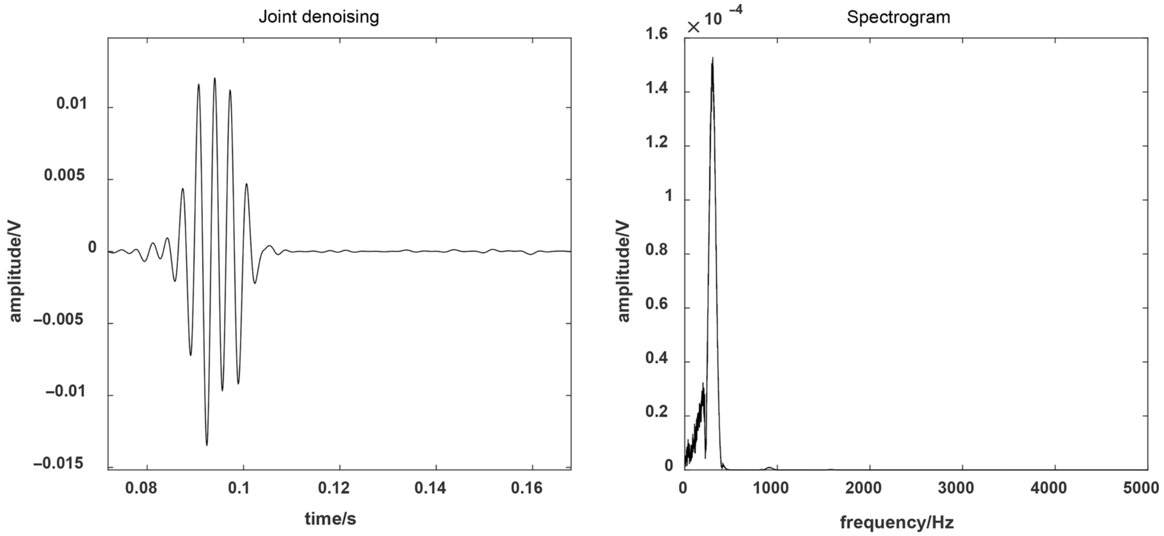

Source: Created by authors

Figure 23 DOA estimation results after denoising signal

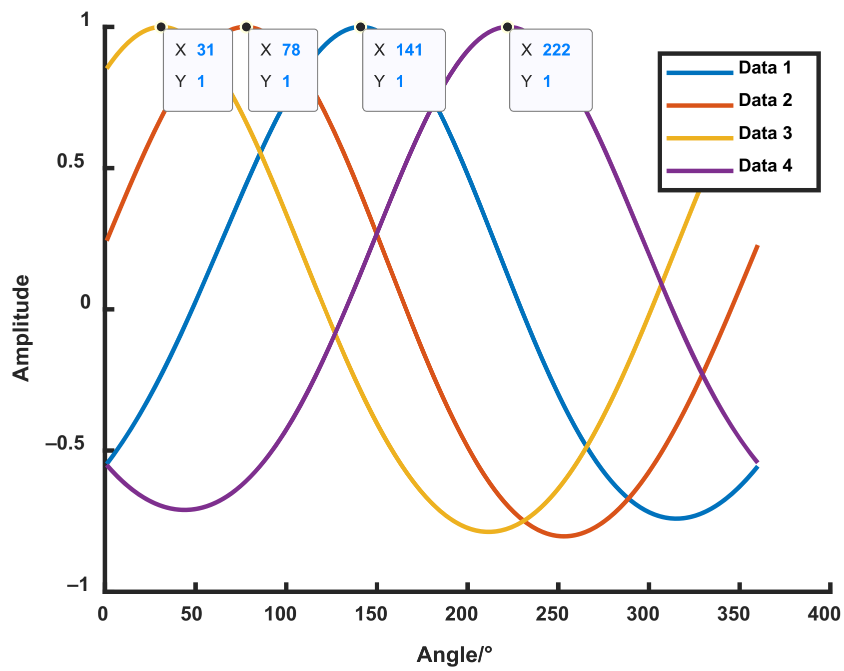

Source: Created by authors

both indoors and outdoors, we verified the feasibility of this algorithm under strong interference from ocean noise. In complex outdoor environments, high-precision azimuth estimation was achieved with an azimuth error of less than 3°. Additionally, the research methodology presented in this paper involves minimal iterations and short processing times, making it convenient for hardware circuit implementation and holding engineering significance. Future work will involve conducting more experiments to identify potential algorithmic issues, further improving the algorithm and develop the hardware circuit for widespread use in underwater acoustic applications.

Figure 24 Azimuth plot of relative angle over time

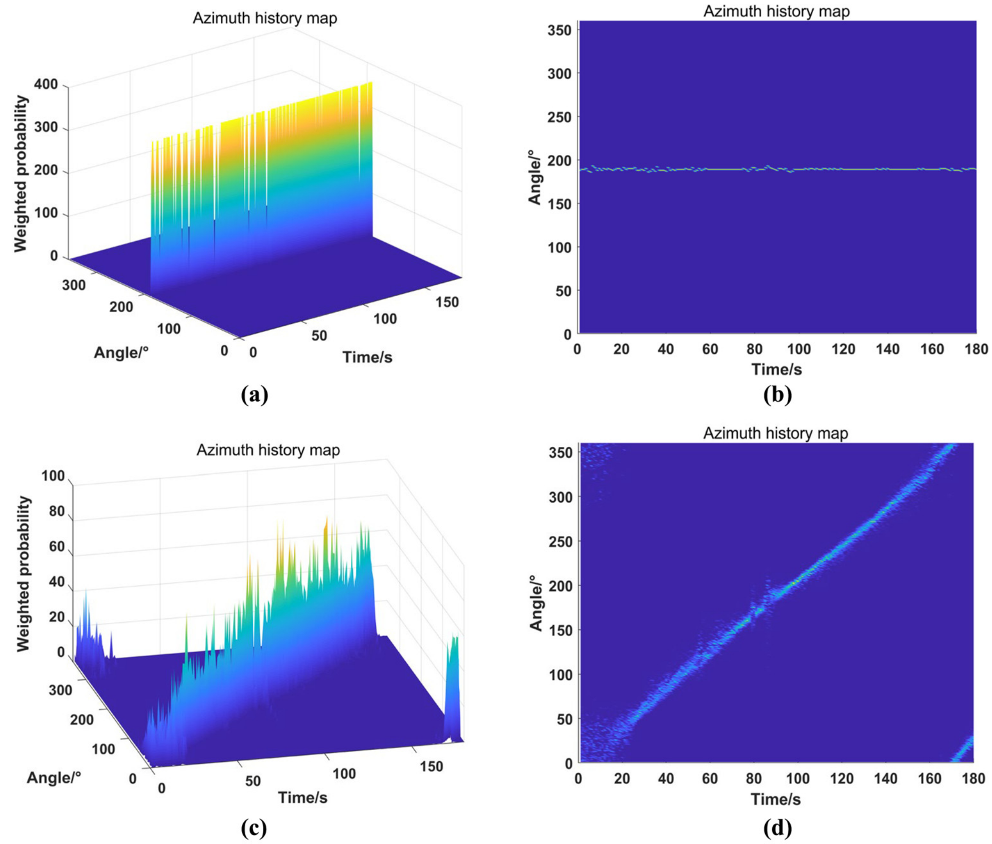

Notes: (a, b) Original signal azimuth diagram; (c, d) Joint denoised signal azimuth diagram
Source: Created by authors

References

Al-Alaoui, M.A. (2007), "Linear phase low-pass IIR digital differentiators", *IEEE Transactions on Signal Processing*, Vol. 55 No. 2, pp. 697-706, doi: 10.1109/tsp.2006.885741.

Cai, J.H. (2019), "Gear fault diagnosis based on a new wavelet adaptive threshold de-noising method", *Industrial Lubrication and Tribology*, Vol. 71 No. 1, pp. 40-47, doi: 10.1108/ilt-03-2018-0101.

Colominas, M.A., Schlotthauer, G. and Torres, M.E. (2014), "Improved complete ensemble EMD: a suitable tool for biomedical signal processing", *Biomedical Signal Processing and Control*, Vol. 14, pp. 19-29, doi: 10.1016/j.bspc.2014.06.009.

Du, X.H., Shuai, W. and Juan, Z. (2017), "Research on marine photovoltaic power forecasting based on wavelet transform and echo state network", *Polish Maritime Research*, Vol. 24 No. s2, pp. 53-59, doi: 10.1515/pomr-2017-0064.

Ferguson, B.G. and Speechley, G.C. (2009), "Acoustic detection and localization of a turboprop aircraft by an array of hydrophones towed below the sea surface", *IEEE Journal of Oceanic Engineering*, Vol. 34 No. 1, pp. 75-82, doi: 10.1109/joe.2008.2011173.

Gao, J.J., Shen, X.H., Zhao, R.Q., Mei, H.D. and Wang, H.Y. (2017), "A double rate localization algorithm with one anchor for multi-hop underwater acoustic networks", *Sensors*, Vol. 17 No. 5, p. 984, doi: 10.3390/s17050984.

Geng, Y.N., Ren, W.R., Zhang, G.J., Chen, P., Zhu, S., Zhang, Y.F. and Zhang, W.D. (2023), "Design and fabrication of hollow Mushroom-Like cilia MEMS vector hydrophone", *IEEE Transactions on Instrumentation and Measurement*, Vol. 72, pp. 1-8, doi: 10.1109/tim.2022.3224998.

Hu, Y.J., Ouyang, Y., Wang, Z.L., Yu, H.Y. and Liu, L. (2023), "Vibration signal denoising method based on CEEMDAN and its application in brake disc unbalance detection", *Mechanical Systems and Signal Processing*, Vol. 187, p. 109972, doi: 10.1016/j.ymssp.2022.109972.

Hu, H., Zhang, L., Yan, H., Bai, Y. and Wang, P. (2019), "Denoising and baseline drift removal method of MEMS hydrophone signal based on VMD and wavelet threshold processing", *IEEE Access*, Vol. 7, pp. 59913-59922, doi: 10.1109/access.2019.2915612.

Jia, L., Zhang, G.J., Zhu, S., Wu, D.Y., Ren, W.R., Geng, Y.N. and Zhang, W.D. (2023), "Direction of arrival estimation for single microelectromechanical systems vector hydrophone using modified wavelet packet De-Noising", *IEEE Sensors Journal*, Vol. 23 No. 12, pp. 13165-13174, doi: 10.1109/jsen.2023.3269857.

Jiang, S.Y., Zhang, X.X., Mo, Y. and Huang, Y.J. (2024), "Research on noise reduction method of underwater acoustic signal based on CEEMDAN Decomposition-

Improved wavelet threshold", *Journal of Physics: Conference Series*, Vol. 2718 No. 1, doi: 10.1088/1742-6596/2718/1/012078.

Johansson, H. (2012), "Fractional-Delay and supersymmetric Mth-Band Linear-Phase FIR filters utilizing partially symmetric and antisymmetric impulse responses", *IEEE Transactions on Circuits and Systems II: Express Briefs*, Vol. 59 No. 6, pp. 366-370, doi: 10.1109/tcsii.2012.2195060.

Li, H.Y., Wang, C.J. and Zhao, D. (2018), "Filter bank properties of envelope modified EMD methods", *IET Signal Processing*, Vol. 12 No. 7, pp. 844-851, doi: 10.1049/iet-spr.2017.0399.

Liu, L.X., Zhang, W.D., Zhang, G.J. and Xue, C.Y. (2014), "Package optimization of the cilium-type MEMS bionic vector hydrophone", *IEEE Sensors Journal*, Vol. 14 No. 4, pp. 1185-1192, doi: 10.1109/jsen.2013.2293669.

Luo, J.P., Liang, X.D., Guo, Q.C., Zhang, L.Q. and Bu, X.X. (2023), "Combined improved CEEMDAN and wavelet transform sea wave interference suppression", *Remote Sensing*, Vol. 15 No. 8, p. 2007, doi: 10.3390/rs15082007.

Luo, S.X., Zhang, M.L., Nie, Y.M., Jia, X.A., Cao, R.H., Zhu, M.T. and Li, X.J. (2022), "Forecasting of monthly precipitation based on ensemble empirical mode decomposition and Bayesian model averaging", *Frontiers in Earth Science*, Vol. 10, p. 926067, doi: 10.3389/feart.2022.926067.

Qu, J.L., Wang, X.F., Gao, F., Zhou, Y.P. and Zhang, X.Y. (2014), "Noise assisted signal decomposition method based on complex empirical mode decomposition", *Acta Physica Sinica*, Vol. 63 No. 11, doi: 10.7498/aps.63.110201.

Shang, Z.Z., Yang, L.B., Zhang, W.D., Zhang, G.J., Zhang, X.Y., Kou, H.R. and Xue, X. (2023), "Combined noise reduction and DOA estimation algorithm for MEMS vector hydrophone based on variational mode decomposition", *Sensor Review*, Vol. 43 No. 2, pp. 99-107, doi: 10.1108/sr-08-2022-0300.

Shang, Z.Z., Zhang, W.D., Zhang, G.J., Zhang, X.Y., Zhang, L.S. and Wang, R.X. (2020), "A study on MEMS vector hydrophone and its orientation algorithm", *Sensor Review*, Vol. 40 No. 2, pp. 191-201, doi: 10.1108/sr-05-2019-0120.

Siddagangaiah, S., Li, Y.A., Guo, X.J., Chen, X., Zhang, Q.F., Yang, K.D. and Yang, Y.X. (2016), "A complexity-based approach for the detection of weak signals in ocean ambient noise", *Entropy*, Vol. 18 No. 3, p. 101, doi: 10.3390/e18030101.

Wu, D.Y., Zhang, G.J., Zhu, S., Liu, Y., Liu, G.C., Jia, L. and Zhang, W.D. (2023), "A baseline drift removal algorithm based on cumulative sum and downsampling for hydroacoustic signal", *Measurement*, Vol. 207, p. 112344, doi: 10.1016/j.measurement.2022.112344.

Wu, Y.D., Zhang, W.D., Wu, D.Y., Zhu, S., Liu, Y., Jia, L. and Zhang, G.J. (2024), "A directional algorithm from single MEMS vector hydrophone based on polynomial fitting and real-time attitude compensation", *Measurement*, Vol. 227, p. 114195, doi: 10.1016/j.measurement.2024.114195.

Yang, X., Xu, Q.D., Zhang, G.J., Zhang, L.S., Wang, W.D., Shang, Z.Z. and Zhang, W.D. (2021), "Design and implementation of hollow cilium cylinder MEMS vector hydrophone", *Measurement*, Vol. 168, p. 108309, doi: 10.1016/j.measurement.2020.108309.

Zhang, G.J., Zhang, L.S., Ji, S.X., Yang, X., Wang, R.X., Zhang, W.D. and Yang, S. (2021), "Design and implementation of a composite hydrophone of sound pressure and sound pressure gradient", *Micromachines*, Vol. 12 No. 8, p. 939, doi: 10.3390/mi12080939.

Zhang, W.D., Guan, L.G., Zhang, G.J., Xue, C.Y., Zhang, K.R. and Wang, J.P. (2009), "Research of DOA estimation based on single MEMS vector hydrophone", *Sensors*, Vol. 9 No. 9, pp. 6823-6834, doi: 10.3390/s90906823.

Zhu, S., Zhang, G.J., Shang, Z.Z., Yang, X., Lv, T., Liang, X.Q. and Zhang, W.D. (2021), "Design and realization of cap-shaped cilia MEMS vector hydrophone", *Measurement*, Vol. 183, p. 109818, doi: 10.1016/j.measurement.2021.109818.

Zhu, S., Zhang, G.J., Wu, D.Y., Liang, X.Q., Zhang, Y.F., Lv, T. and Zhang, W.D. (2022), "Research on direction of arrival estimation based on self-Contained MEMS vector hydrophone", *Micromachines*, Vol. 13 No. 2, p. 236, doi: 10.3390/mi13020236.

Corresponding author

Guojun Zhang can be contacted at: zhangguojun1977@nuc.edu.cn